Hindawi
Advances in Polymer Technology
Volume 2021, Article ID 4343241, 10 pages
https://doi.org/10.1155/2021/4343241

Research Article

Facile Production of Graphene/Polypropylene Composites with Enhanced Electrical and Thermal Properties through In Situ Artificial Latex Preparation

Lijing Han,[1] Hairui Wang,[1] Yingxia Zong,[2] and Chengzhong Zong[1]

[1]*School of Polymer Science and Engineering, Qingdao University of Science and Technology, Qingdao 266042, China*
[2]*College of Chemical and Molecular Engineering, Qingdao University of Science and Technology, Qingdao 266042, China*

Correspondence should be addressed to Yingxia Zong; 4017020039@mails.qust.edu.cn

Received 7 June 2021; Revised 12 August 2021; Accepted 27 August 2021; Published 11 December 2021

Academic Editor: Kinga Pielichowska

In order to obtain the unique properties of graphene-based composites, to realize homogeneous dispersion of graphene throughout the polymer matrix remains the key challenge. In this work, edge-oxidized graphene/polypropylene (EOGr/PP) composites with well-dispersed EOGr in PP matrix, synchronously exhibiting high electrical conductivity and thermal property, were simply fabricated for the first time using a novel strategy by in situ artificial PP latex preparation in the presence of EOGr based on solution-emulsification technique. The good dispersion state of EOGr in the PP matrix was demonstrated by means of X-ray diffraction (XRD), transmission electron microscopy (TEM), and scanning electron microscopy (SEM). A blue shift in Raman G peak of the EOGr nanosheets was observed in the EOGr/PP composites, indicating the strong interactions between the EOGr nanosheets and the PP matrix. The onset crystallization and crystallization peak temperatures increased as the EOGr loading increases due to its good nucleating ability. An improved thermal stability of EOGr/PP composites was observed as evaluated by TGA. The EOGr/PP composites showed an insulator-to-conductor percolation transition in between that of 1 and 2 wt% EOGr content. Such strategy provides a very effective pathway to fabricate high-performance nonpolar polymer/graphene composites with excellent dispersion state of graphene.

1. Introduction

Polypropylene (PP) is one of the most common thermoplastics which has been widely used in many fields. Recently, graphene/PP composites have emerged as an appealing material fulfilling the requirements of many practical applications owing to the enhanced mechanical as well as other physical properties (electrical conductivity, thermal conductivity, barrier property, etc.). One of the major challenges in the preparation of graphene/PP composites is to realize the homogeneous and uniform dispersion of graphene nanosheets in PP matrix because the interaction between the two materials is rather weak [1, 2], which would result in predominant graphene aggregation. In recent reports, melt mixing technique is the most common method for the preparation of such materials [3, 4]. However, melt mixing process has several drawbacks including generally poor dispersion of graphene in the PP matrix and risk of degradation of polymer chains during the process, resulting in the fact that it is very difficult to produce high-performance graphene/PP composites. Solution mixing is an effective way to achieve a homogeneously dispersed graphene in polymer [5–7]. However, for nonpolar polymer PP, graphene cannot disperse homogeneously in the solvent that can dissolve PP completely, such as xylene [8], so that solution mixing technique becomes impossible to prepare nanoscale dispersed graphene/PP composites.

Recently, a versatile and environment-friendly latex technology has been utilized to fabricate polymeric nanocomposites based on carbon nanotubes and graphene [9, 10]. By blending a carbon nanotube/graphene dispersion in water with a polymer emulsion, composites with excellent filler distribution and dispersion can be achieved. The key to produce graphene/PP composites through latex blending

is to secure the cellular morphology and perform a high-level reduction of GO. There are two main strategies reported in the literature: (i) GO is blended with the PP latex followed by reduction to restore the basal plane of graphene [11], or (ii) RGO or pristine FLG is blended with the PP latex [12], *i.e.*, the reduction step occurs prior to the blending step. Each strategy has advantages and drawbacks. On the one hand, GO is hydrophilic and can be dispersed in water, resulting in the fact that GO nanosheets can be easily mixed with the PP latex leading to a stable suspension; therefore, graphene/PP composite fabrication through latex blending may be a rather straightforward process. However, the reduction step is critical, which has a great influence on suspension stability, morphology control, and reduction efficiency. During the reduction step, hydrophilic GO became hydrophobic RGO tending to destabilize the suspension as a result of the disappearance of oxygen-containing groups. The existence of PP latex particles can hardly prevent the aggregating of RGO due to the lack of strong interaction between PP latex and GO, so the RGO distribution and the cellular morphology have to be secured during this step. Moreover, Wang et al. [13] prepared the RGO/PP composites by mixing the PP latex with an exfoliated GO aqueous dispersion and a subsequent in situ chemical reduction of GO in the presence of hydrazine hydrate. Raman spectrum analysis demonstrated that the presence of the PP latex gave rise to a slight decrease in the reduction efficiency of GO nanosheets. On the other hand, using directly RGO or pristine FLG prevents the need for a reduction step, but they are not stable in water without the aid of stabilizers, which makes it difficult to prepare a stable suspension and secure the composite morphology.

Furthermore, to the best of our knowledge, in all reports on the preparation of graphene/PP composites through latex blending, the used PP latex is water-based emulsion of maleic-anhydride-grafted-isotactic polypropylene (PP-g-MA) with relatively low molecular weight as the matrix because the production of PP in aqueous dispersion is limited due to the need of water-sensitive catalysts.

In order to obtain graphene/PP composites with enhanced mechanical and thermal properties, Song et al. [14] successfully fabricated graphene/PP masterbatch by blending PP latex with an exfoliated GO aqueous dispersion and subsequently reducing the GO nanosheets, which can be further melt blended with PP matrix. However, there still exist some graphene aggregations in as-prepared composites. Maybe it is because that at high GO loading, van der Waals force makes reduced GO sheets easily aggregate during the reduction step, even if subsequent melt blending cannot redisperse aggregated RGO in the PP matrix.

In this paper, we reported for the first time a novel strategy for the preparation of graphene/PP composites through latex technology. The graphene/PP composites were produced through in situ artificial PP latex preparation based on solution-emulsification technique where the organic phase of PP in cyclohexane was added to the aqueous phase of emulsifiers and graphene in deionized water with vigorous agitation. In order to avoid the reduction of GO nanosheets, in our strategy, the used graphene was edge-oxidized multilayer graphene (EOGr) exhibiting both high conductivity and high dispersibility. The strong interactions between EOGr nanosheets and PP matrix taking place through the bridging of emulsifiers made EOGr nanosheets prefer adsorbing onto the surface of PP latex particles, facilitating the uniform dispersion of EOGr throughout PP matrix. Both the electrical conductivity and thermal stability of the obtained EOGr/PP composites were improved remarkably by introducing EOGr. The preparation of an artificial polymer latex in the presence of graphene provides a promising approach to produce high-performance nonpolar polymer composites with graphene as the nanofiller.

2. Experimental Section

2.1. Raw Materials. Sodium persulfate ($Na_2S_2O_8$), ferrous sulfate ($FeSO_4{\cdot}7H_2O$), cetyl alcohol (1-hexadecanol) (CA), and cyclohexane were purchased from Sinopharm and used as received. Highly conductive multilayer graphene (pristine graphene, PG) was supplied by Qingdao ENE-carbon real new materials Tech. Co. Ltd., China. Potassium oleate and hexadecyltrimethoxysilane (HDMS) were purchased from Macklin. Polyethylene-block-poly (ethylene glycol) (PE-b-PEG, Mw 1400, PE/PEG 1 : 1 by weight) was purchased from Sigma-Aldrich. Polypropylene (PP 4220, melt flow index: 0.45 g/10 min) is a copolymer of propylene, and ethylene and was purchased from Sinopec Yanshan Petrochemical Company.

2.2. Fabrication of Edge-Oxidized Multilayer Graphene (EOGr). EOGr with both high conductivity and dispersibility was prepared from highly conductive multilayer graphene (PG) by an edge-oxidation strategy based on oxidizing radicals ($SO_4^{-\bullet}$) and the detailed preparation procedures and characterization data could be found in our previous report [15]. Briefly, after 30 g $Na_2S_2O_8$ was added into a 500 mL round-bottomed flask with a mixture of deionized water (200 mL) and PG (300 mg), the mixed solution was continuously stirred and simultaneously purged with ultrapure nitrogen to remove dissolved oxygen and carbon dioxide. After 15 min, 100 mL of 1 mol L^{-1} $FeSO_4$ solution was added into the flask with continuous drip addition through a constant pressure funnel in 24 h at 25°C. Then, the obtained products were washed with deionized water repeatedly until the filtrate became neutral. Finally, EOGr aqueous dispersion (solid content 0.1%) was obtained by sonicating at 480 W for 1 h.

2.3. Preparation of EOGr/PP Composites. In the first step, PP 4220 was added into cyclohexane and stirred gently at 85°C until a clear solution was obtained. Then, PE-b-PEG and HDMS were added and stirred gently for another 2 h, thereby obtaining the organic phase. The EOGr aqueous dispersion was mixed with the aqueous solution of potassium oleate and then sonicated for 1 h. Next, CA was added into the mixture and stirred for 2 h at 70°C to promote the dissolution of CA, thereby obtaining the aqueous phase. The recipes for organic and aqueous phases can be shown in Tables 1 and 2. In the second step, the organic phase was

Table 1: Recipes for the aqueous phase of solution-emulsification.

Aqueous phase	1	2	3
Potassium oleate (g)	1	1	1
EOGr aqueous dispersion (g)	10	20	40
CA (g)	0.02	0.02	0.02
Deionized water (g)	90	80	60

Table 2: Recipe for the organic phase of solution-emulsification.

Organic phase	
PP4220 (g)	2
PE-b-PEG (g)	0.1
HDMS (g)	0.1
Cyclohexane (g)	98

cooled down to 70°C and then added into the aqueous phase slowly through a glass dropper with vigorous stirring at 70°C for 2 h to form a stable crude emulsion. Next, the obtained crude graphene/PP latex was further stirred gently in a flask with reflux condensation for 8 h. In the last step, cyclohexane was removed by distillation under vacuum at 50°C. Then, alcohol was poured into the as-prepared EOGr/PP latex quickly under vigorous stirring to get the precipitation of the EOGr/PP composites, which were isolated by vacuum filtration and washed with plenty of deionized water and alcohol repeatedly. The obtained EOGr/PP-x composites were vacuum dried at 70°C for 24 h and directly hot pressed at 10 MPa for 10 min. Herein, x represented the EOGr content as parts per hundred parts of PP, set to be 0.5, 1, and 2 phr in the composites.

2.4. Characterization. A Renishaw InVia Reflex Raman system with 512 nm IR-diode laser coupled to an optical microscope was used to record spectra from the samples. X-ray diffraction (XRD) was carried out using a Rigaku X-ray generator from 2θ values ranging from 5 to 30° at room temperature. Transmission electron microscopy (TEM) images were obtained using a JEM-2100 instrument at an acceleration voltage of 200 kV. The composite sample was obtained by freezing ultrathinned sectioning with a thickness of ~100 nm. Scanning electron microscopy (SEM) images were obtained using a JSM-7500F instrument operating at 20 kV. The fracture surfaces of the EOGr/PP composites were obtained by quenching in liquid nitrogen and then coated with a thin layer of gold using a sputtering coater for SEM observation. Fourier transform infrared spectroscopy (FT-IR) was recorded by a Bruker Vertex 70 FT-IR spectrometer with the scan range of 400-4000 cm^{-1} in ATR mode. For neat PP and EOGr/PP-0.5 samples, the resistance was measured with a high-resistance instrument (Beijing Huace Testing Equipment Co. Ltd, China). In the case of EOGr/PP-1 and EOGr/PP-2 samples, the resistance was determined using a Keithley 2636B system source-meter. The measured volume resistance (Ω), R_v was converted to bulk conductivity with the following equation: $\sigma_v = L/(R_v \cdot S)$, where L is specimen thickness and S is the effective area of the measuring electrode. Thermogravimetric analysis (TGA) was carried out by using an TG209F1 instrument under a nitrogen flow (20 mL/min) with a temperature range of 30-600°C (heating rate 10°C/min). Differential scanning calorimeter (DSC) was used for investigating the crystallization using a nonisothermal 10°C/min cooling ramp.

3. Results and Discussion

3.1. Fabrication of EOGr/PP Composites. To obtain the unique properties of graphene-based composites, the uniform dispersion of graphene throughout the polymer matrix is critical. In order to fabricate well-dispersed EOGr/PP composites through latex technology, a novel strategy by in situ artificial PP latex preparation based on the solution-emulsification technique in the presence of EOGr was employed for the first time and the schematic representation of fabricating the composites is presented in Scheme 1. The used EOGr was edge-oxidized multilayer graphene exhibiting high dispersibility due to the oxygen-containing groups at the edge of the graphene and high conductivity because edge-oxidation did not evidently compromise the crystal structure of graphene. Therefore, unlike previous latex technology for the preparation of graphene/PP composites, the reduction step was not required in our strategy.

To fabricate a stable EOGr/PP latex, the most important factor is the choice of the emulsifying system. In our strategy, the emulsifying system: ionic surfactant (potassium oleate), nonionic surfactant (PE-b-PEG), cosurfactant (HDMS), stabilizer (EOGr), and costabilizer (CA), was employed. The PE-b-PEG is a block copolymer, and its structure is $H_3CH_2C(CH_2CH_2)_{25}(OCH_2CH_2)_{16}OH$. The PE block is compatible with the organic phase due to the fact that the structure and property of PE are similar with the PP matrix, and the PEG block is highly compatible with the aqueous phase in the middle temperature (50-80°C) [16]. Han et al. [17] have found that 3-aminopropyltriethoxysilane (APES) and tetraethyl orthosilicate (TEOS) may possess some emulsification and played the cosurfactant role in the emulsification process. According to this result, it is reasonable to infer that hexadecyltrimethoxysilane (HDMS) may play a similar emulsification. Kuziel et al. [18] demonstrated the true amphipathic nature of pristine graphene flakes and predicted that graphene flakes can be efficiently used as a new-generation stabilizer. We speculate that EOGr nanosheets are 2D amphiphiles with well-defined hydrophobic and hydrophilic regions: the basal plane and oxidized edges, and can play a stabilizer role in the emulsification process. Cetyl alcohol (CA), a highly water-insoluble long-chain fatty alcohol was used as a costabilizer retarding the emulsion degradation due to the slow polymer diffusion rate from small to larger particles [19].

3.2. Morphology Analysis. X-ray diffraction (XRD) measurement is usually utilized to gain insight into the dispersion state of graphene within the polymer matrix by monitoring the 2θ position, shape, and intensity of the (002) diffraction peak from the distributed graphene layers. As shown in Figure 1, the XRD profile of EOGr showed a broad peak

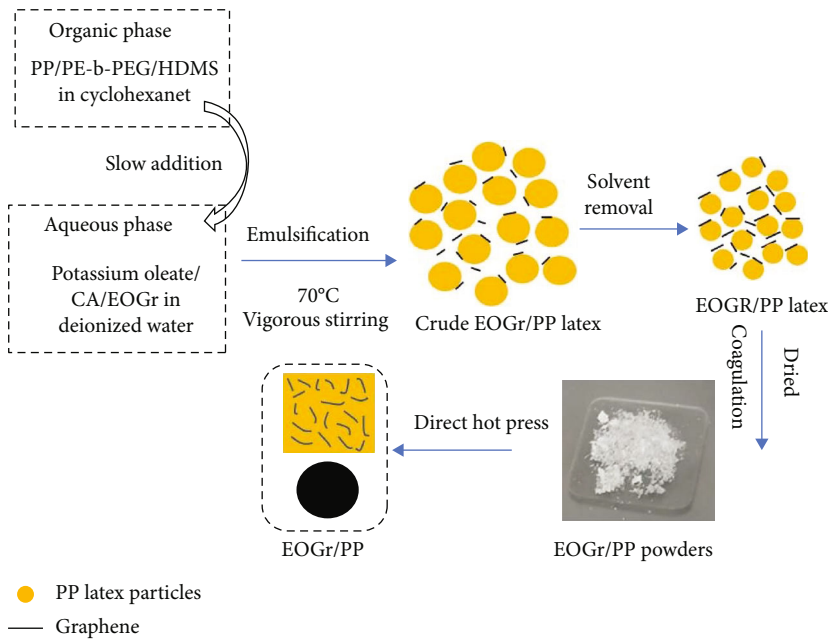

Scheme 1: Schematic representation of the preparation of EOGr/PP composites by latex technology.

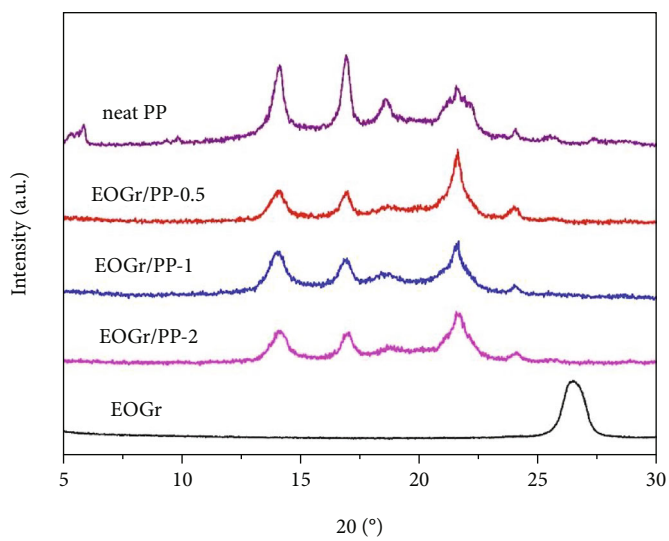

Figure 1: X-ray diffraction patterns for EOGr, neat PP, and the EOGr/PP composites with different contents of EOGr.

centered at about 26.5° (d_{002}), indicating that the aggregation of EOGr nanosheets occurred due to the strong van der Waals' forces in the interlayer. However, in the XRD profiles of the EOGr/PP composites with different EOGr contents, no diffraction peaks were observed except the crystalline diffraction peaks of the PP matrix. The absence of EOGr diffraction peak in the investigated EOGr/PP composite samples could be a sign that the homogenous dispersion of EOGr nanosheets in the PP matrix was possibly achieved. The characteristic diffraction peaks at $2\theta = 14.1°$, 16.9°, 18.6°, and 21.6° are corresponding to the (110), (040), (130), and (111) + (041) crystalline planes of α-form PP, respectively. The peak shape and intensity change at 14.1, 16.9, and 18.6 of the PP matrix in the presence of EOGr was readily observed, indicating that the introduction of EOGr affected the crystallization behavior of the PP matrix to some extent. This effect of EOGr on the crystallization of the PP matrix is later investigated using DSC analysis and discussed in the following paragraph.

The results provided only by XRD measurements cannot determine the spatial distribution of the EOGr nanosheets in the PP matrix, although the disappearance of EOGr diffraction peak in XRD scans is observed. In order to visualize the dispersion of EOGr nanosheets in the PP matrix and to support the interpretation of XRD profiles, TEM investigations were performed. Figure 2(a) shows the TEM micrograph of

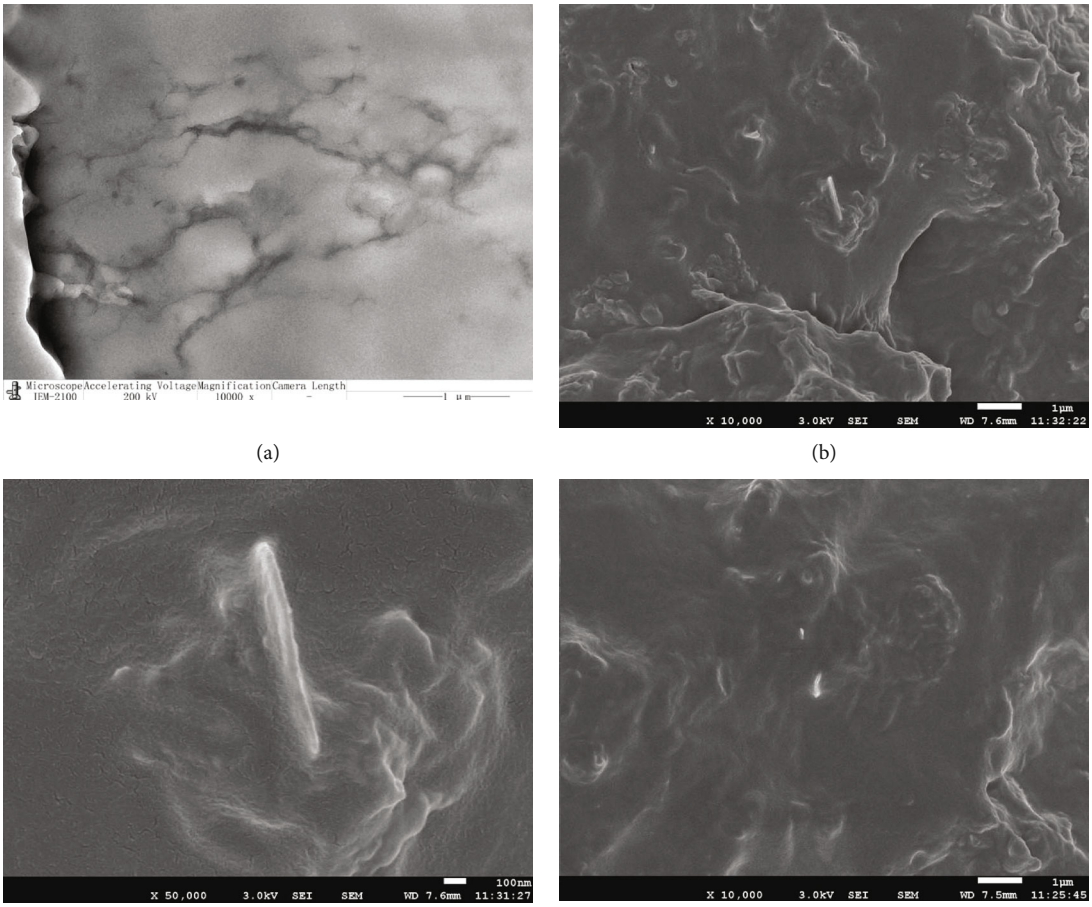

(a) (b)

(c) (d)

Figure 2: (a) TEM image of the EOGr/PP composite with 1 wt% EOGr and SEM images of the EOGr/PP composite with 1 wt% EOGr (b) and 2 wt% EOGr (c). (b′) Is the magnified image of (b).

EOGr nanosheets in the PP matrix at an EOGr loading of 1 wt%. While XRD data indicated the homogenous dispersion of EOGr nanosheets in the PP matrix (absence of EOGr characteristic peak), some stacks of EOGr layers were still found in TEM image, not indicating the aggregation of EOGr during the preparation process due to the multilayer structure of EOGr itself. According to the observation from TEM and XRD analysis, EOGr nanosheets were dispersed uniformly throughout the PP matrix without significant aggregation by in situ artificial PP latex preparation.

SEM analysis was employed to get a peek into the morphology of EOGr/PP composites. Figure 2(b) shows the SEM image of the fracture surface of the EOGr/PP composite with an EOGr concentration of 1 wt% after hot-press molding. It can be clearly seen that EOGr nanosheets were homogeneously dispersed in the PP matrix with an extremely low concentration of aggregation, and the fracture surface was smooth without any EOGr pulled out. This may be a result of the strong interactions between the EOGr nanosheets and the PP matrix, possibly taking place through the bridging of emulsifiers (PE-b-PEG and HDMS). The H-bonding interaction was formed between PEG block ($-OCH_2CH_2-$) of PE-b-PEG and hydroxy (-OH) functionality of HDMS hydrolysate and edge functionalities of EOGr. Also, the hydrophobic parts of PE-b-PEG and HDMS are alkyl chains which are compatible with the PP matrix due to the similar structure. The presence of the strong interactions made EOGr nanosheets prefer adsorbing onto the surface of the PP latex particles rather than aggregation with each other. Moreover, during drying and hot press, the abundant H-bonding interaction can be transformed into covalently bonded structure through thermally induced condensation and simultaneous conversions of -COOH (EOGr) ....HO- (PEG block) to ester (-C(= O)O-), HO-C (EOGr) ....HO-C (PEG block) to C-O-C, or HO-C (EOGr) ....HO-Si (HMDS hydrolysate) to C-O-Si. Therefore, in this work, high-performance EOGr/PP composites without discernible EOGr aggregation can be achieved.

Fourier transform infrared spectroscopy (FT-IR) was employed to investigate the molecular-level interaction between EOGr sheets and PP latex particles. For comparison, the PP latex without EOGr was prepared through the same procedures, followed by coagulation and drying. The obtained sample was designated as PP latex particle. The FT-IR spectra of EOGr, PP latex particle, and EOGr/PP-2 composite are presented in Figure 3. The spectrum of EOGr

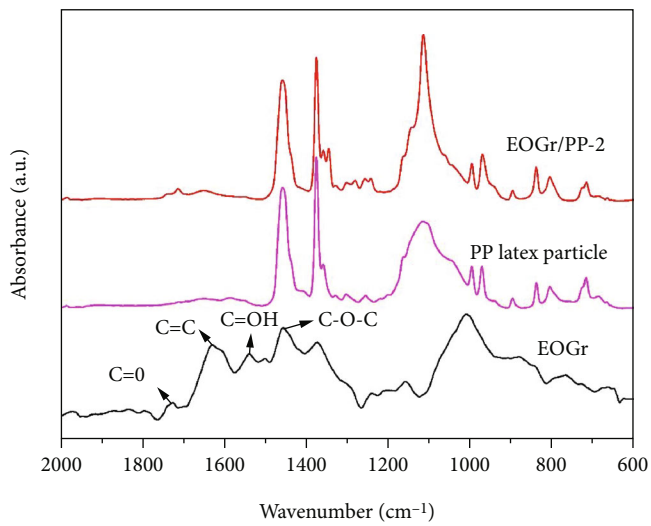

Figure 3: FT-IR spectra of EOGr, PP latex particle, and EOGr/PP-2.

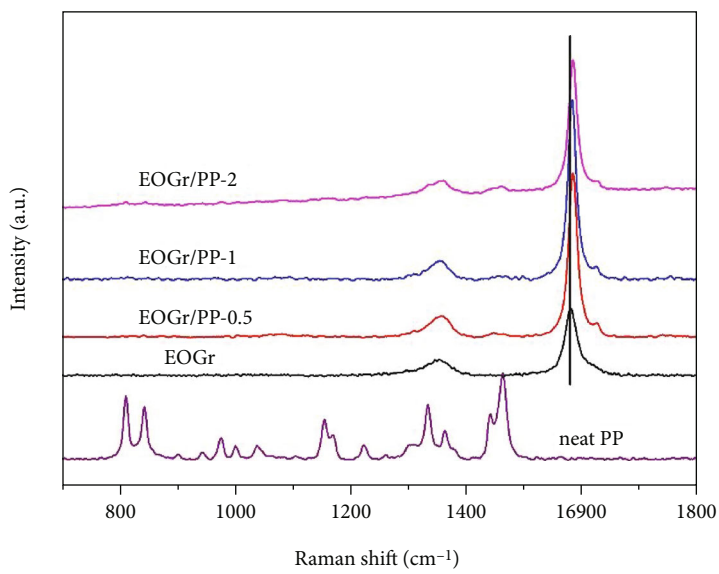

Figure 4: Raman spectra of EOGr, neat PP, and the EOGr/PP composites with different contents of EOGr.

showed an absorption peak at 1730 cm^{-1} due to the C=O stretching of the -COOH group. It also exhibited absorption peaks at 1625, 1537, and 1450 cm^{-1} attributed to C=C, C-O-H, and C-O-C bonds. For the PP latex particle, the characteristic absorption peak at around 1110 cm^{-1} is assigned to the stretching vibrations of C-O-C or Si-O-Si bonds. For the EOGr/PP-2 composite, the absorption peak of C=O stretching at 1730 cm^{-1} for EOGr was slightly shifted towards lower energy which may be due to the H-bonded -COOH. Compared to that of the PP latex particle, the peak at ~1110 cm^{-1} became stronger which may be due to the formation of C-O-C or C-O-Si bonds.

The strong interactions between the EOGr nanosheets and the PP matrix were also confirmed by using Raman spectroscopy because it monitors the D peak (~1350 cm^{-1}) and G peak (~1580 cm^{-1}, the in-plane vibration adsorption of sp^2 graphitic structure) of graphene. As shown in Figure 4, two characteristic peaks of EOGr were observed at 1577 cm^{-1} and 1349 cm^{-1}. By comparing the G-peak positions of EOGr and EOGr/PP composites, it can be seen that the G-peak positions of EOGr/PP composites were stiffened (i.e., shifted to higher frequencies) by ~6 cm^{-1} in relation to those of EOGr, which indicated the structural changes that occurred in EOGr [20]. In this study, the blue shift of G peak suggested that strong interfacial interactions existed between the EOGr nanosheets and PP chains.

3.3. Thermal Properties of EOGr/PP Composites. In order to quantify the effects of EOGr nanosheets on the crystallization behavior of PP matrix, the nonisothermal crystallization tests from the melt at a cooling rate of 10°C/min were carried out. As shown in Figure 5(a), the addition of EOGr into the PP matrix led the crystallization of the EOGr/PP composites to start at higher temperatures as compared to that of the

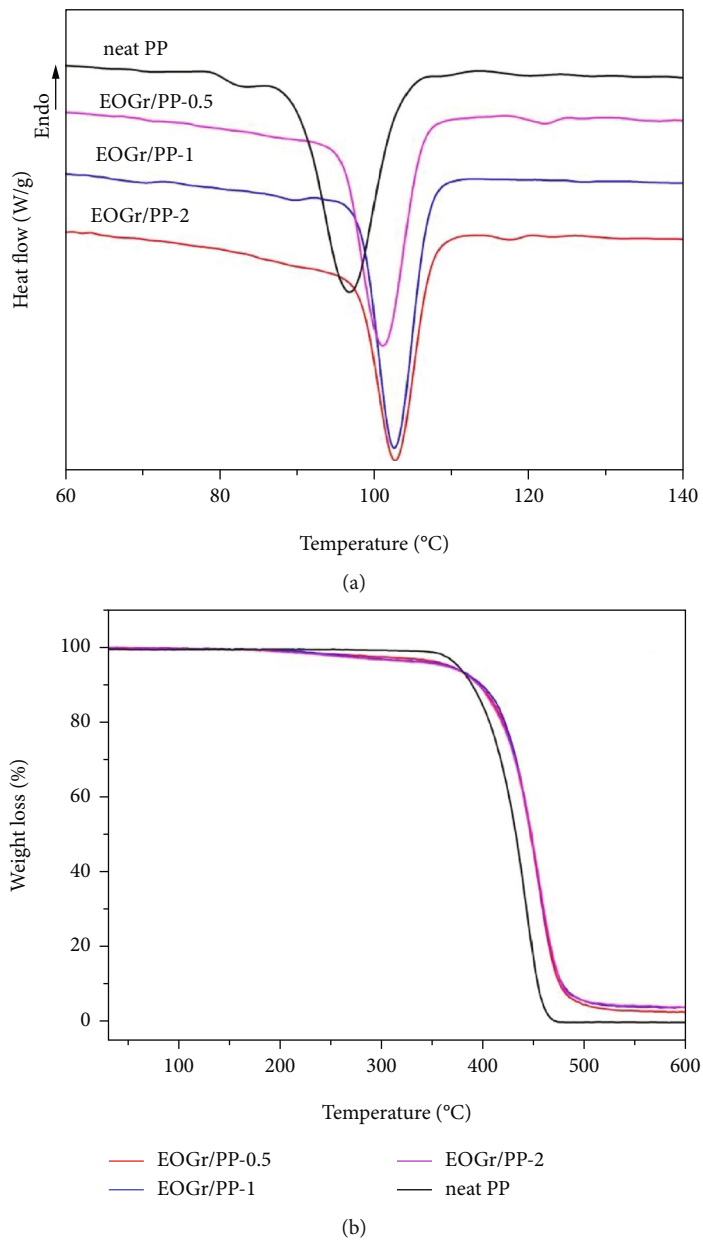

Figure 5: DSC curves (a) and TGA curves (b) of neat PP and EOGr/PP composites with different contents of EOGr.

neat PP, and the crystallization peak temperatures of the EOGr/PP composites were also observed to significant increase. In all the EOGr/PP composites, both the onset crystallization and crystallization peak temperatures followed an increasing trend with the increase of EOGr concentration. For example, the crystallization peak and onset crystallization temperatures of EOGr/PP-2 composite were found to be 5.9°C and 4.5°C higher than those of neat PP, respectively (see Table 3). These findings demonstrated the capability of EOGr nanosheets to speed up the kinetics of the crystallization process of the PP matrix mainly due to the strong heterogeneous nucleation effect of EOGr nanosheets [21]. However, George et al. [11] observed that the presence of RGO resulted in wider and shallower crystallization (exothermic) curves, while in our EOGr/PP systems, the presence of EOGr did not show such an effect. This discrepancy in the crystallization behavior may be due to the difference in the kind of PP resin and graphene and the preparation method.

TGA was carried out in nitrogen atmosphere to study the thermal stability of neat PP and EOGr/PP composites, presented in Figure 5(b). It can be clearly seen that the maximum weight loss temperatures (T_{max}) of the EOGr/PP composites were both shifted up to higher temperatures compared to those of neat PP, suggesting a significant improvement of the thermal stability of the EOGr/PP composites as compared to that of neat PP (see Table 3). The thermal stability of the EOGr/PP composites increased by

Table 3: Onset crystallization, crystallization peak and mass loss temperatures for neat PP and EOGr/PP composites.

Sample	Crystallization peak temperature (°C)	Onset crystallization temperature (°C)	Weight loss temperature (°C)			
			1%	2%	3%	Maximum
Neat PP	96.8	106.3	335	359	365	443
EOGr/PP-0.5	101.0	109.2	203	268	325	454
EOGr/PP-1	102.5	110.6	216	256	288	455
EOGr/PP-2	102.7	110.8	197	245	284	457

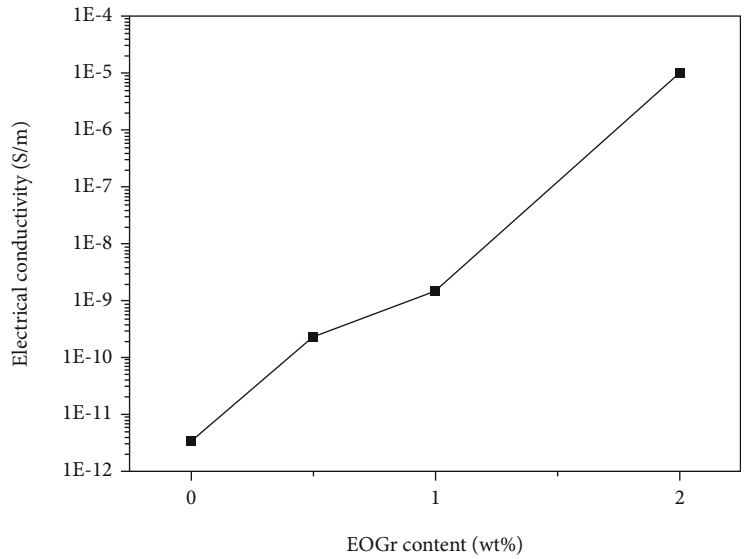

Figure 6: Electrical conductivity of neat PP and EOGr/PP composites with different contents of EOGr.

about 12°C upon the introduction of EOGr compared to neat PP. However, it was worth pointing out that the TGA curves of EOGr/PP composites were found to have evident weight loss in the range between 250 and 300°C, which were attributed to the loss of oxygen-containing groups on the EOGr sheets and the PEG block of PE-b-PEG. Similar phenomenon has also been observed in other graphene/polymer composites [22]. The EOGr with lamellar structure homogeneously dispersed in the polymer matrix could provide a physical barrier effect leading to an enhanced decomposition temperature [23]. Therefore, the incorporation of EOGr can improve the thermal stability of the PP matrix.

3.4. Electrical Property of EOGr/PP Composites. It is well-known that the dispersion state of graphene throughout the polymer matrix plays an important role in the electrical conductivity of composites [24]. Figure 6 shows the electrical conductivity variation of neat PP and the EOGr/PP composites as a function of EOGr mass fraction. The electrical conductivity of EOGr/PP composites increased with increasing EOGr loading, which is attributed to the gradual emergence of continuous conductive pathways/networks throughout the PP matrix facilitating the current transfer. The critical amount of conductive filler required to cause the insulator-to-conductor transition is known as the percolation threshold. At concentrations between 1 and 2 wt%, the electrical conductivity increased drastically from 1.5×10^{-9} to 1.3×10^{-5} S/m, revealing that for the present system, the percolation threshold of conductivity is between 1 wt% and 2 wt% EOGr loading. The low percolation threshold indicated that the uniform distribution of EOGr throughout the PP matrix was achieved, facilitating the formation of conductive networks/pathways in the composites. To conclude, our novel strategy by in situ artificial PP latex preparation to produce EOGr/PP composites can efficiently suppress the aggregation of EOGr, resulting in a relatively high electrical conductivity.

4. Conclusions

In this work, we reported for the first time a novel strategy for the preparation of EOGr/PP composites through in situ artificial PP latex preparation in the presence of EOGr based on the solution-emulsification technique. The EOGr/PP composites with well-dispersed EOGr nanosheets throughout the PP matrix were successfully fabricated and investigated by XRD, SEM, and TEM. Moreover, Raman analysis suggested that strong interactions existed between EOGr nanosheets and PP matrix, facilitating the uniform dispersion morphology of EOGr in PP. Calorimetric investigations showed that the EOGr/PP composites exhibited increment in onset crystallization and crystallization peak temperatures due to the nucleating ability of EOGr. Increased thermal stability of the EOGr/PP composites compared to neat PP in

inert atmosphere was revealed by TGA. The EOGr/PP composites also exhibited relatively high electrical conductivity with a percolation threshold in between 1 and 2 wt%. Such strategy provides a very effective pathway to fabricate high-performance nonpolar polymer/graphene composites with excellent dispersion state of graphene.

Data Availability

The data used to support the findings of this study are included within the article.

Conflicts of Interest

The authors declare that they have no conflicts of interest.

Authors' Contributions

Lijing Han was responsible for conceptualization, methodology, validation, formal analysis, and writing original draft. Hairui Wang was responsible for formal analysis and visualization. Chengzhong Zong was responsible for writing, review, and editing. Yingxia Zong was responsible for writing, review, and English language editing of our revised manuscript. All authors have read and agreed to the published version of the manuscript.

Acknowledgments

This work was supported by the Natural Science Foundation of Shandong Province (project No. ZR2020QE072).

References

[1] C. Lv, Q. Xue, D. Xia, M. Ma, J. Xie, and H. Chen, "Effect of chemisorption on the interfacial bonding characteristics of graphene–polymer composites," *Journal of Physical Chemistry C*, vol. 114, no. 14, pp. 6588–6594, 2010.

[2] F. E. Alam, W. Dai, M. Yang et al., "In situ formation of a cellular graphene framework in thermoplastic composites leading to superior thermal conductivity," *Journal of Materials Chemistry A. Materials*, vol. 5, no. 13, pp. 6164–6169, 2017.

[3] M.-C. Hsiao, S. H. Liao, Y. F. Lin et al., "Preparation and characterization of polypropylene-graft-thermally reduced graphite oxide with an improved compatibility with polypropylene-based nanocomposite," *Nanoscale*, vol. 3, no. 4, pp. 1516–1522, 2011.

[4] K. Kalaitzidou, H. Fukushima, and L. T. Drzal, "Mechanical properties and morphological characterization of exfoliated graphite–polypropylene nanocomposites," *Composites. Part A, Applied Science and Manufacturing*, vol. 38, no. 7, pp. 1675–1682, 2007.

[5] S. Stankovich, D. A. Dikin, G. H. B. Dommett et al., "Graphene-based composite materials," *Nature*, vol. 442, no. 7100, pp. 282–286, 2006.

[6] J. Liang, Y. Huang, L. Zhang et al., "Molecular-level dispersion of graphene into poly(vinyl alcohol) and effective reinforcement of their nanocomposites," *Advanced Functional Materials*, vol. 19, no. 14, pp. 2297–2302, 2009.

[7] P. Chammingkwan, K. Matsushita, T. Taniike, and M. Terano, "Enhancement in mechanical and electrical properties of polypropylene using graphene oxide grafted with end-functionalized polypropylene," *Materials*, vol. 9, no. 4, p. 240, 2016.

[8] J. I. Paredes, S. Villar-Rodil, A. Martínez-Alonso, and J. M. D. Tascón, "Graphene oxide dispersions in organic solvents," *Langmuir: the ACS Journal of Surfaces and Colloids*, vol. 24, no. 19, pp. 10560–10564, 2008.

[9] E. Tkalya, M. Ghislandi, A. Alekseev, C. Koning, and J. Loos, "Latex-based concept for the preparation of graphene-based polymer nanocomposites," *Journal of Materials Chemistry*, vol. 20, no. 15, p. 3035, 2010.

[10] O. Regev, P. N. B. ElKati, J. Loos, and C. E. Koning, "Preparation of conductive nanotube–polymer composites using latex technology," *Advanced Materials*, vol. 16, no. 3, pp. 248–251, 2004.

[11] G. George, S. M. Simon, P. V. P. et al., "Green and facile approach to prepare polypropylene/in situreduced graphene oxide nanocomposites with excellent electromagnetic interference shielding properties," *RSC Advances*, vol. 8, no. 53, pp. 30412–30428, 2018.

[12] J. Cao, X. Zhang, X. Wu, S. Wang, and C. Lu, "Cellulose nanocrystals mediated assembly of graphene in rubber composites for chemical sensing applications," *Carbohydrate Polymers*, vol. 140, pp. 88–95, 2016.

[13] D. Wang, X. Zhang, J. W. Zha, J. Zhao, Z. M. Dang, and G. H. Hu, "Dielectric properties of reduced graphene oxide/polypropylene composites with ultralow percolation threshold," *Polymer*, vol. 54, no. 7, pp. 1916–1922, 2013.

[14] P. Song, Z. Cao, Y. Cai, L. Zhao, Z. Fang, and S. Fu, "Fabrication of exfoliated graphene-based polypropylene nanocomposites with enhanced mechanical and thermal properties," *Polymer*, vol. 52, no. 18, pp. 4001–4010, 2011.

[15] L. Han, Y. Zong, Q. Tang et al., "Green and facile edge-oxidation of multi-layer graphene by sodium persulfate activated with ferrous ions," *RSC Advances*, vol. 10, no. 51, pp. 30716–30722, 2020.

[16] L. Zu, R. Li, L. Jin, H. Lian, Y. Liu, and X. Cui, "Preparation and characterization of polypropylene/silica composite particle with interpenetrating network via hot emulsion sol–gel approach," *Progress in Natural Science*, vol. 24, no. 1, pp. 42–49, 2014.

[17] L. Han, C. Gao, X. Wu et al., "Anionic surfactants templating route for synthesizing silica hollow spheres with different shell porosity," *Solid State Sciences*, vol. 13, no. 4, pp. 721–728, 2011.

[18] A. W. Kuziel, K. Z. Milowska, P. L. Chau et al., "The true amphipathic nature of graphene flakes: a versatile 2D stabilizer," *Advanced Materials*, vol. 32, no. 34, article 2000608, 2020.

[19] D. L. Tillier, J. Meuldijk, and C. E. Koning, "Production of colloidally stable latices from low molecular weight ethylene–propylene–diene copolymers," *Polymer*, vol. 44, no. 26, pp. 7883–7890, 2003.

[20] M. C. Hsiao, S. H. Liao, M. Y. Yen et al., "Preparation of covalently functionalized graphene using residual oxygen-containing functional groups," *ACS Applied Materials & Interfaces*, vol. 2, no. 11, pp. 3092–3099, 2010.

[21] S. Zhao, F. Chen, C. Zhao, Y. Huang, J. Y. Dong, and C. C. Han, "Interpenetrating network formation in isotactic polypropylene/graphene composites," *Polymer*, vol. 54, no. 14, pp. 3680–3690, 2013.

[22] L. Zhang, T. Shi, S. Wu, and H. Zhou, "Graphene/polystyrene nanocomposites synthesized via Pickering emulsion polymerization," *High Performance Polymers*, vol. 26, no. 2, pp. 156–165, 2013.

[23] C. Feng, H. Ni, J. Chen, and W. Yang, "Facile method to fabricate highly thermally conductive graphite/PP composite with network structures," *ACS Applied Materials & Interfaces*, vol. 8, no. 30, pp. 19732–19738, 2016.

[24] Y. Huang, Y. Qin, Y. Zhou, H. Niu, Z. Z. Yu, and J. Y. Dong, "Polypropylene/graphene oxide nanocomposites prepared by in situ Ziegler–Natta polymerization," *Chemistry of Materials*, vol. 22, no. 13, pp. 4096–4102, 2010.